JOURNAL OF SOLID STATE CHEMISTRY 44, 212–229 (1982)

Nonstoichiometry and Defects in V_9O_{17}

HIROSHI SATO, NOBUO OTSUKA, HIDEHIKO KUWAMOTO,* AND G. L. LIEDL

School of Materials Engineering, Purdue University, West Lafayette, Indiana 47907

Received February 1, 1982; in revised form April 27, 1982

Defects associated with nonstoichiometry in the Magnéli-phase compounds V_nO_{2n-1} were investigated by transmission electron microscopy in the composition range mainly between V_9O_{17} and VO_2. Involvement of excess oxygen in the Magnéli-phase structures beyond strict stoichiometry, especially beyond V_9O_{17}, tends to create planar defects which are almost parallel to but are inclined slightly from the (011) plane of the VO_2 structure, crossing the (121) *CS* planes. These defects subsequently tend to form microtwin bands with ordered (132) *CS* planes. Differences in behavior between the V–O system and Ti–O system with respect to the formation of long-period structures are discussed in this connection.

Introduction

The existence of a series of homologous, long-period compounds V_nO_{2n-1} $(3 \leq n \leq 9)$ has been known for some time, and their crystal structure has been investigated in detail for $n = 3$ to $n = 7$ (*1*). The structure is basically a periodic modulation of VO_2 having the rutile structure: one oxygen layer is removed at every nth V layer in the direction perpendicular to the (121) plane of VO_2. The (121) plane, where one oxygen layer is missing, is called the crystallographic shear (*CS*) plane and is the site for compensation of the nonstoichiometry (or the deviation of the ratio of V to O from 1 : 2) of these compounds. The V_nO_{2n-1} phases themselves are sometimes called nonstoichiometric compounds and the meaning of the word nonstoichiometry is not necessarily clear. However, in this study the word nonstoichiometry is utilized to indicate either an excess or deficit in constituent ions with respect to fully compensated composition of a certain reference structure.

There have been several efforts to determine if any long-period structures exist beyond V_9O_{17} (*2–5*). We investigated this situation in detail in connection with the effort to grow single-phase single crystals of V_9O_{17} (*5*). Although we observed the existence of $V_{10}O_{19}$ and of some longer-period compounds of the same symmetry which were found intergrown microsyntactically with V_9O_{17} grown under highly nonequilibrium conditions, we could confirm that V_9O_{17} is the long-period limit among the Magnéli-phase compounds under the equilibrium condition and that no equilibrium phase exists in the composition range between V_9O_{17} and VO_2 (*5*). Therefore, our interest is to determine, by high-resolution

* Present address: Rockwell International Science Center, Thousand Oaks, California 91360.

0022-4596/82/110212-18$02.00/0

transmission electron microscopy, how the Magnéli-phase compounds compensate for nonstoichiometry by mechanisms other than the (121) *CS* planes when excess oxygen ions are incorporated into V_9O_{17}.

In the Ti–O system the existence of the Magnéli-phase compounds Ti_nO_{2n-1} ($4 \leq n \leq 10$) of the same structure (*6*) has also been documented and investigated extensively by transmission electron microscopy (*2*). In this system, different from the V–O system, the existence of another series of homologous compounds with similar structures beyond $Ti_{10}O_{19}$ has been established (*7*). In the composition range between $TiO_{1.933}$ and $TiO_{1.98}$, a series of homologous compounds of the same formula, Ti_nO_{2n-1} ($12 \leq n \leq 36$, even n) with the (132) *CS* planes, is found.[1] In addition, between the two homologous series, many intermediate phases with periodic *CS* planes, again with the formula Ti_nO_{2n-1}, exist.[2] In addition to these compounds, the *CS* planes lie between the (121) and the (132) planes and they change from the (121) to the (132) orientation as the oxygen concentration increases (*2*). In other words, in the Ti–O system the nonstoichiometry beyond the long-period limit $Ti_{10}O_{19}$ of the Magnéli phase is still accommodated by formation of *CS* planes which are different from the (121) orientation. The investigation of the V–O system beyond V_9O_{17} is thus expected to contribute to the understanding of the difference in the two systems with respect to the formation of long-period compounds.

[1] The lower limit of n seems to depend on the condition of preparation (*2*). Recently, Bando *et al.* (*8*) successfully grew single crystals of this series of compounds from $Ti_{16}O_{31}$ to $Ti_{20}O_{39}$, except $Ti_{19}O_{37}$. The existence of a compound with odd n in this series of compounds had not been known previously.

[2] Structures in this range are considered to be transitions from the structures with the (121) *CS* planes and those with the (132) *CS* planes and are more generally represented by the formula Ti_nO_{2n-p} ($p \neq 1$) with integral values of n rather than as mixtures of the two typical structures.

Experimental Procedures

Specimens were prepared first in a powder form by reacting a mixture of V_2O_3 and V_2O_5 powder at 900°C for 3 days. The composition of the powder specimen nominally corresponded to $V_{10}O_{19}$. Crystals were then grown from the powder specimen by means of a chemical vapor transport technique utilizing $TeCl_4$ as a transport agent. The growth condition was the same as that for growing stoichiometric V_9O_{17} single crystals reported earlier (*5*). Single crystals of compounds V_nO_{2n-1} from $n = 6$ to $n = 8$ were also grown for comparison from reacted powders with compositions corresponding to V_6O_{11}, V_7O_{13}, and V_8O_{15}, respectively.

Grown crystals were crushed in an agate mortar and fine, crushed pieces were mounted on carbon films for TEM observation. Specimens for high-resolution observation were mounted on carbon-coated microgrids instead of carbon films. A JEM 200 CX electron microscope with a side entry goniometer was used for observation. The microscope has a resolution of 3.0 Å under the axial illumination condition.

Results

Specimens grown from powder having the nominal composition $V_{10}O_{19}$ consist of single crystals of either V_9O_{17} or VO_2, but small V_8O_{15} single crystals are also occasionally found among these. Any intergrowth of other phases, either macroscopic or microscopic, in these crystals is not observed, and both diffraction patterns and lattice images indicate the presence of periodic arrays of *CS* planes. This implies that the growth condition in these specimens approached that of growing single-phase single crystals of V_9O_{17} (*5*), but the oxygen content in these specimens during the growth and possibly also in the final state is in excess of that in V_9O_{17}.

Some diffraction patterns taken of these V_9O_{17} crystals reveal distinctive streaks. The existence of such distinctive streaks has never been found in V_9O_{17} grown from powders having the stoichiometric composition. An example of diffraction patterns showing such streaking is given in Fig. 1a. The beam orientation is in the $[1\bar{1}1]$ direction.[3] Here, the 121 and the 011 reflections correspond to the 009 and 010 reflections based on the unit cell of V_nO_{2n-1} first defined by Horiuchi *et al.* (*1*). Streaks are parallel to the $[011]^*$ direction and are apparent both at strong and at weak spots. Diffraction patterns taken with various beam orientations show that these streaks are due to one-dimensional diffuse scattering which is parallel to the $[011]^*$ axis. This means that the streaks are due to planar faults lying on the (011) plane.

Figure 1b is the lattice image of the area producing the diffraction pattern in Fig. 1a. The beam orientation is the same as that of the diffraction pattern. The image reveals a group of parallel, planar defects crossing the (121) *CS* planes along the (011) plane. In the orientation shown in Fig. 1a, the planar faults are perpendicular to the image plane. Wide areas between defects show regular arrangements of V_9O_{17} crystal with the (121) *CS* planes with a 14.4-Å interval. On the other hand, images of the *CS* planes are severely distorted in areas where defects are closely collected. These planar defects have various widths: the thinnest probably consists of one atomic plane, while thicker ones have widths of a few tens of angstroms. It is also seen that thick defects located at the left side of the image in Fig. 1b have internal structures. Ordered fringes, similar to those due to the *CS* planes but with orientation different from those of the (121) *CS* planes, are observed inside.

[3] Indices are referred to the tetragonal rutile structure in this paper. The relation between these and the indices based on the unit cell defined by Horiuchi *et al.* is given in Ref. (*5*).

Lattice images of more than 30 areas of the V_9O_{17} crystals were observed with the beam in the $[1\bar{1}1]$ orientation. Defects are found in most areas. On the other hand, in "stoichiometric" V_9O_{17} or in any V_nO_{2n-1} ($n < 9$) crystals similarly prepared earlier (*5*) such a high density of defects was not observed. These specimens were practically free of the (011) defects. Therefore, this type of defect is considered to be related to the involvement of excess oxygen beyond V_9O_{17} as discussed in more detail later. Aggregations of defects are observed whenever streaks appear in corresponding diffraction patterns, but even if streaks in the diffraction pattern are not detected, some isolated defects of this kind still occur.

In addition to the features stated earlier, some thin defects are found to have kinks. An example of such a kink is shown by the arrow in Fig. 1b. In other words, these defects involve steps which are parallel to the $[1\bar{1}1]$ direction. The existence of a series of such steps tends to bend the defect plane out of the (011) plane. Indeed, bent defects whose orientation deviates from the (011) plane are also observed in some areas. Figure 2 shows such defects. The image was taken with the beam in the $[1\bar{1}1]$ orientation. It is seen that the deviation can occur on either side from the (011) plane. The largest deviation from the (011) plane is about 5°. The angle of deviation is experimentally determined with respect to the (121) *CS* planes. These bent defects are thought to consist of a series of steps. Since defects are inclined to either side of the (011) plane, streaks which appear parallel to the $[011]^*$ direction in the observed diffraction pattern correspond to the average structure of the area.

Figure 3 shows bright-field images of a specimen which has two thin defects in the area the widths of which are a few angstroms, based on the lattice image taken with the beam in the $[1\bar{1}1]$ orientation.

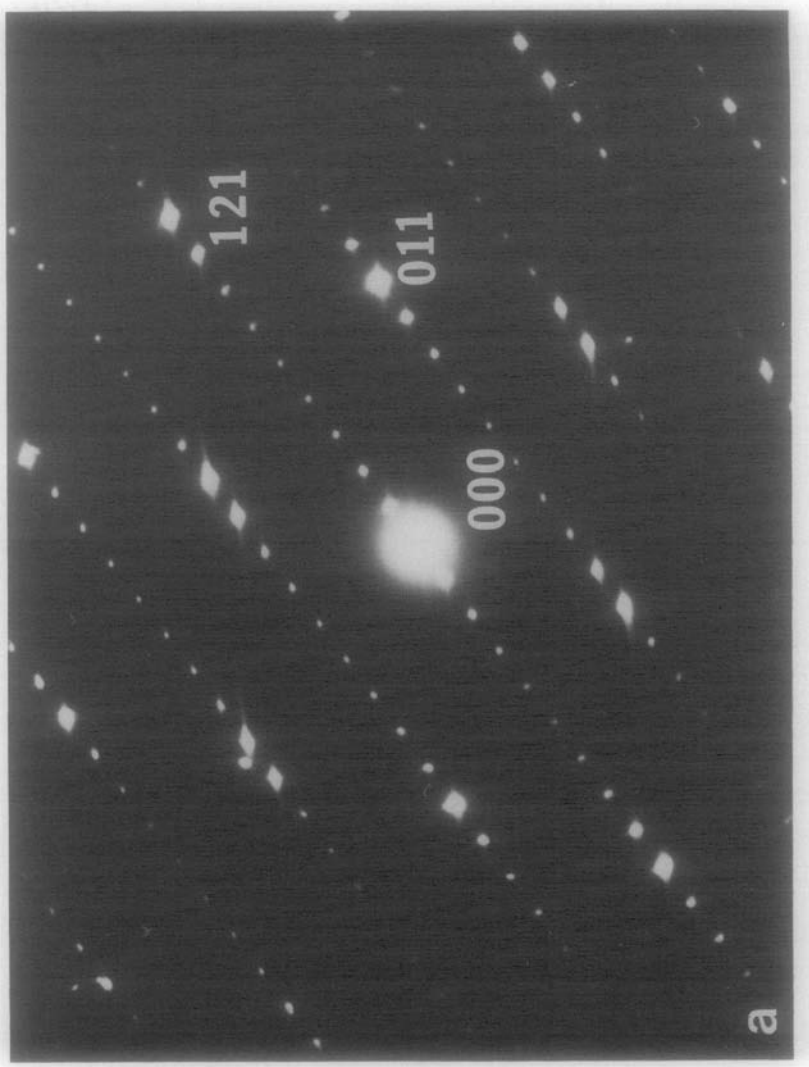

FIG. 1a. Diffraction pattern taken from a V_9O_{17} crystal. The pattern shows streaks in the $[011]^*$ direction.

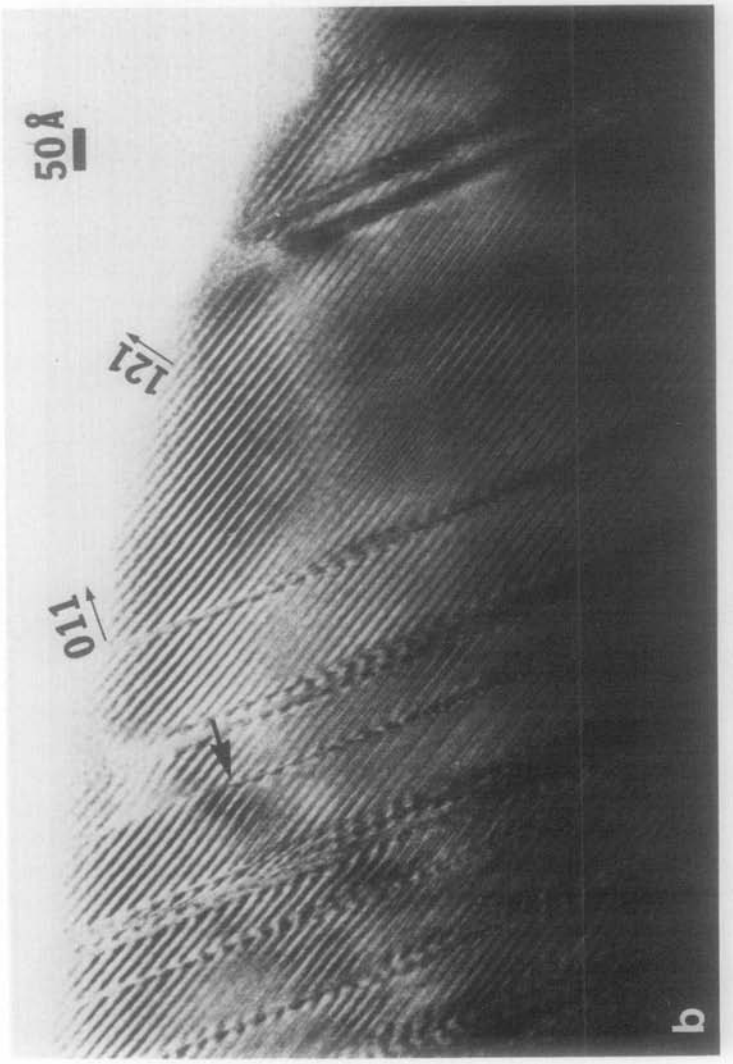

FIG. 1b. Lattice image taken from the area in which the diffraction pattern shown in Fig. 1a is taken. The incidence beam is in the [$1\bar{1}1$] orientation. Thick defects in the left side of the image have an internal structure. A heavy arrow indicates a jog in a defect.

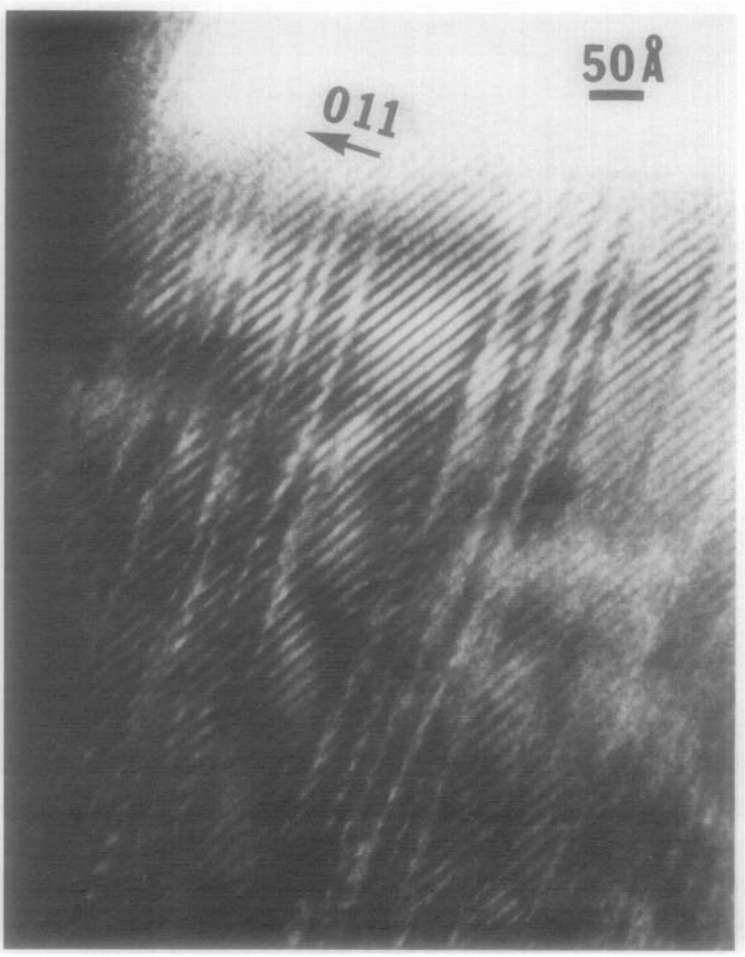

FIG. 2. Lattice image of a V_9O_{17} crystal showing defects whose orientation deviate from the (011) plane. The beam is in the $[1\bar{1}1]$ orientation.

These bright-field images were taken approximately under the two-beam condition, with a Bragg reflection g = 110, 111, and 211, respectively. It can be seen that contours due to the defects appear for g = 110 but almost disappear for cases with g equal to 111 or 211. These extinction conditions indicate that crystals divided by the defect are displaced relative to each other along the $[0\bar{1}1]$ direction which lies in both the (111) and the (211) planes. The $[0\bar{1}1]$ direction also lies in the defect plane.

Figure 4a is a high-resolution image taken from a very thin area of a V_9O_{17} crystal. The image was taken under the axial illumination condition with the beam in the $[1\bar{1}1]$ orientation. The image is taken with about 900 Å underfocusing, close to the optimum defocusing condition in this case. The amount of defocusing is estimated from the width of the Fresnel fringe appearing at the edge of the crystal. Under this condition, the image represents the projection of the actual charge distribution in the crystal. Figure 4b is a schematic diagram of the projection of a V_9O_{17} crystal with the same direction of projection as that of the image in Fig. 4a. Large open and small solid circles

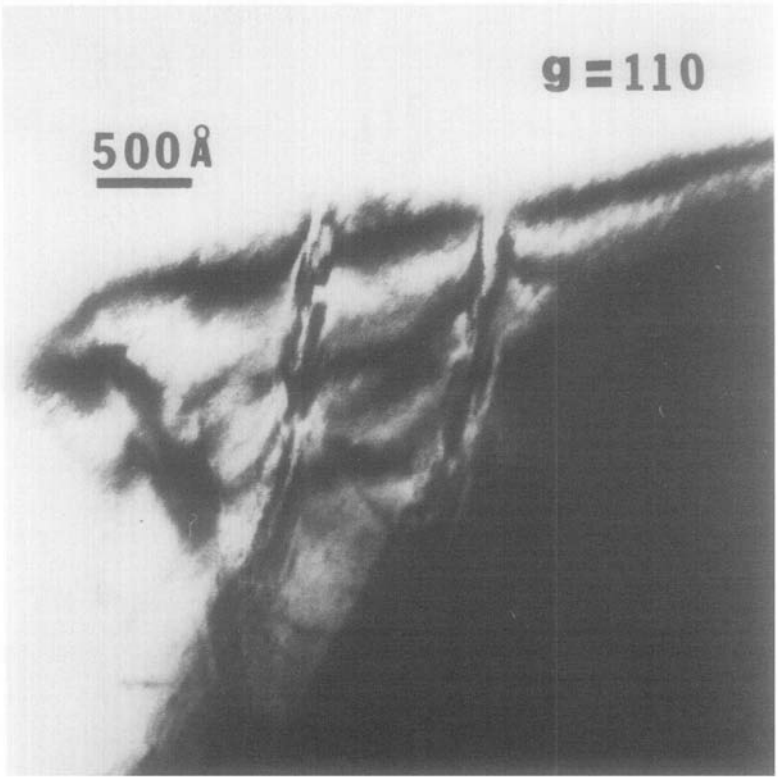

FIG. 3. Bright-field image of a V_9O_{17} crystal showing two (011) defects. The image is taken under the two beam conditions with Bragg reflections g = 110, 111, and 211, respectively.

represent oxygen and metal ions, respectively. *CS* planes are indicated by broken lines. Note the defect which appears in the center of the image in Fig. 4a. It is seen that the *CS* planes as well as (110) lattice fringes (horizontal fringes) change their orientations at the defect line and then return to the original orientations on the other side of the line. This indicates that both sides of the crystal divided by the defect are displaced relative to each other along the defect plane and this observation coincides with the result of the analysis based on the bright-field images in Fig. 3. The image shows that the amount of the displacement across the defect is one and a half times the (110) lattice spacing. On the other hand, the width of the defect is approximately equal to three times the (011) interplanar distance (2.4 Å). Therefore, if the defect consists of three consecutive stacking shifts along the (011) plane, each stacking shift has a displacement vector of $\frac{1}{2}$ [0$\bar{1}$1], based on the VO_2 lattice. Utilizing this concept, the structure of thicker defects can be explained as follows: the thinnest possible defects consist of a single stacking fault with the displacement vector of $\frac{1}{2}$ [0$\bar{1}$1], and thicker defects are a number of consecutive stacking faults on every (011) plane. Figure 5 shows schematically a defect consisting of a single stacking fault. Solid circles here represent the metal ions, and oxygen ions are not shown. A solid line at the center is the stacking fault and broken lines indicate the (121) *CS* planes. The figure shows that the defect in its idealized form is an antiphase boundary with respect to the VO_2 crystal. It should, however, be mentioned that, for creating an antiphase boundary in VO_2, the shift across the boundary can be any odd multiple of the $\frac{1}{2}$ [0$\bar{1}$1] vector. As

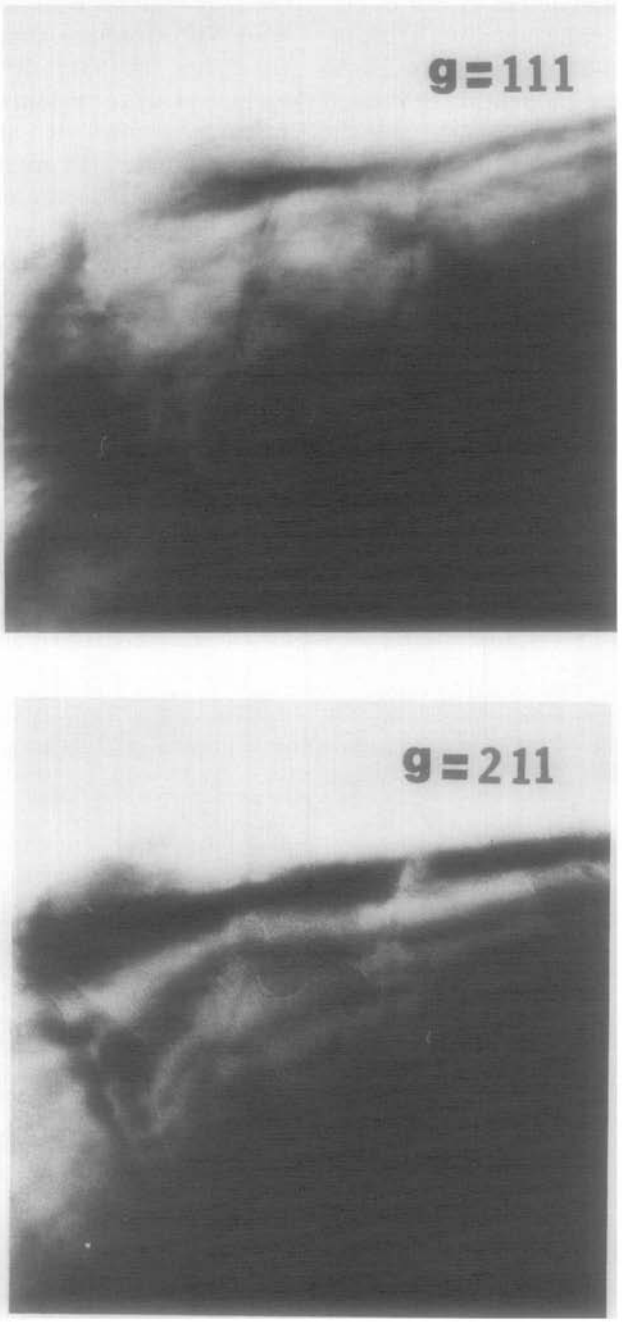

FIG. 3—*Continued.*

shown later, there is evidence that the shift involves a $\frac{1}{2}$ [0$\bar{1}$1] rather than a $\frac{1}{2}$ [0$\bar{1}$1] vector under certain conditions.

Figure 6a is a high-resolution image of a V_9O_{17} crystal showing a thick defect with internal structure and Fig. 6b is the corresponding diffraction pattern. The image was taken under the same defocusing condition

as the image for a thin defect shown in Fig. 4a. The diffraction pattern shows extra intensity maxima in the [011]* streaks. These intensity maxima are thought to be caused by the internal structure of the defect. These look like twin spots of the underlying V_9O_{17} crystal at first sight. However, their positions deviate systematically from those expected from a twin. The direction of a line connecting two adjacent extra spots (indicated by arrows) does not coincide with the [121]* direction of the VO_2 structure of V_9O_{17}. Instead, the direction is parallel to the [132]* axis of the twin. (For the sake of brevity, we call the structure having the twin relation with respect to the underlying VO_2 structure simply as the twin.) In the image, the [121]* direction of the matrix and the [132]* direction of the twin are indicated by arrows. It can be seen that the parallel lines which are perpendicular to the [132]* axis are separated by an interval of about 10 Å and are connected to the (121) *CS* planes in the matrix one by one. The (110) lattice fringes in Fig. 6a also show that the defect is in the twin relation with respect to the matrix of VO_2. These features indicate that the internal structure of the defect which is in a twin relation with the matrix is described as the ordered (132) *CS*

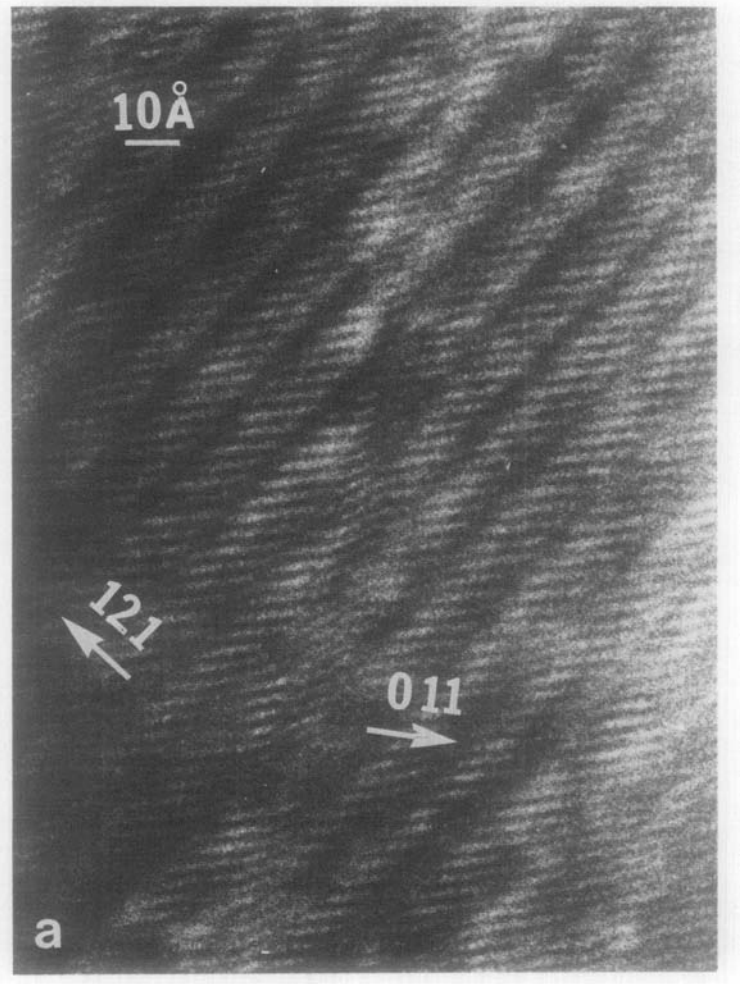

FIG. 4a. High-resolution image of a V_9O_{17} crystal showing a (011) defect.

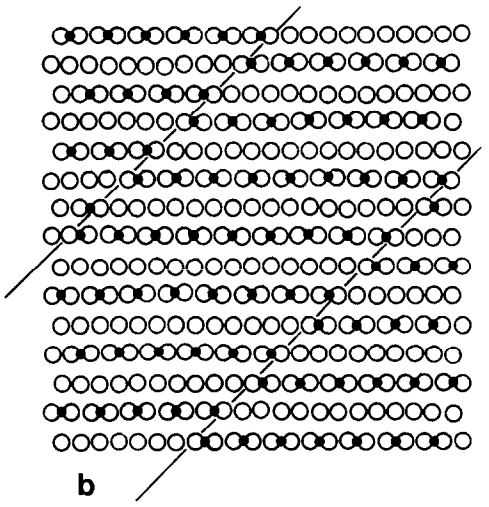

FIG. 4b. Projection of a V_9O_{17} crystal. Large open and small solid circles represent oxygen and metal ions, respectively. The orientation of the projection corresponds to that of the image in (a).

planes. The intensity maxima in the diffraction pattern (Fig. 6b) are thus confirmed to be due to the ordered (132) *CS* planes in the twin. Further, the intensity maxima are always connected with Bragg spots due to the ordered (121) *CS* planes in the matrix by the streaks in the [011]* direction. This means that the distance between the two adjacent (132) *CS* planes along the (011) plane is the same as that between the two adjacent (121) *CS* planes in the [1$\bar{1}$1] projection. Figure 7 schematically shows a projection of a defect (microtwin) having such an internal structure. Solid circles represent vanadium ions and the oxygen ions are not shown. Both the (121) and the (132) *CS* planes indicated by broken lines are connected to one another at the boundaries between the microtwin and the matrix. The figure shows that the period of the ordered (132) *CS* planes is that of V_9O_{17}. In order to create a twin with the ordered (132) *CS* planes shown in Fig. 7, however, the relative shift across each antiphase boundary must be $\frac{7}{2}$ [0$\bar{1}$1] rather than $\frac{1}{2}$ [0$\bar{1}$1].

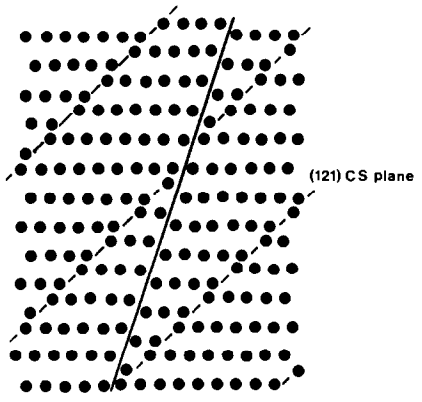

FIG. 5. Structure model of a thin (011) defect. Only metal ions are represented by solid circles. A continuous line at the center is an antiphase boundary and broken lines represent the (121) planes.

It is also observed that a bent antiphase boundary tends to be straightened out by the motion of the jog along the (011) plane. In Fig. 8, an example of such a motion of a jog is shown which occurred during observation. In Fig. 8a, an initial image of a bent defect is shown. In Fig. 8b, an image of the same defect is shown after the motion of the jog. Although not very distinct in this case, such observations indicate that bent antiphase boundaries are created initially during the growth, and that these subsequently decompose into a series of boundaries to form thick defects.

In order to investigate the dependence of the frequency of occurrence of such defects on the period of the structure, the microstructures of V_nO_{2n-1} single crystals from $n = 6$ to $n = 8$ were observed. Lattice images were taken from more than 20 areas of each crystal with the beam in the [1$\bar{1}$1] orientation. In the first place, the occurrence of (011) defect is rare and especially not as distinct in its appearance as those observed in V_9O_{17} studied here. The defects were not encountered at all in V_6O_{11} single crystals but were found occasionally in V_7O_{13} and V_8O_{15} single crystals. Though the result is not fully quantitative, the observation shows that the defect occurs less frequently in V_7O_{13} and V_8O_{15} crystals than in V_9O_{17} crystals. Even in V_9O_{17} crystals, the occurrence of the defects is rare in crystals grown

from the starting material having the stoichiometric composition. However, defects with very large width (twins) were also found in crystals of these compositions. The images of those defects always reveal regularly ordered (132) *CS* planes. Figure 9 exhibits such a defect in a V_7O_{13} crystal. The directions of [121]* and [132]* are indicated by arrows.

Discussion

The present observation reveals the existence of a new type of structural defect in the Magnéli-phase compounds, V_nO_{2n-1}, with the following characteristics.

1. The defect consists essentially of a series of antiphase boundaries along the (011) plane of the underlying VO_2 crystal with the rutile structure and it predominantly exists in V_9O_{17} grown from the starting material having excess oxygen content.

2. Many defects of this type found in V_9O_{17} are curved by the existence of a series of jogs and deviate from the (011) plane. There is some evidence that bent antiphase boundaries are straightened by

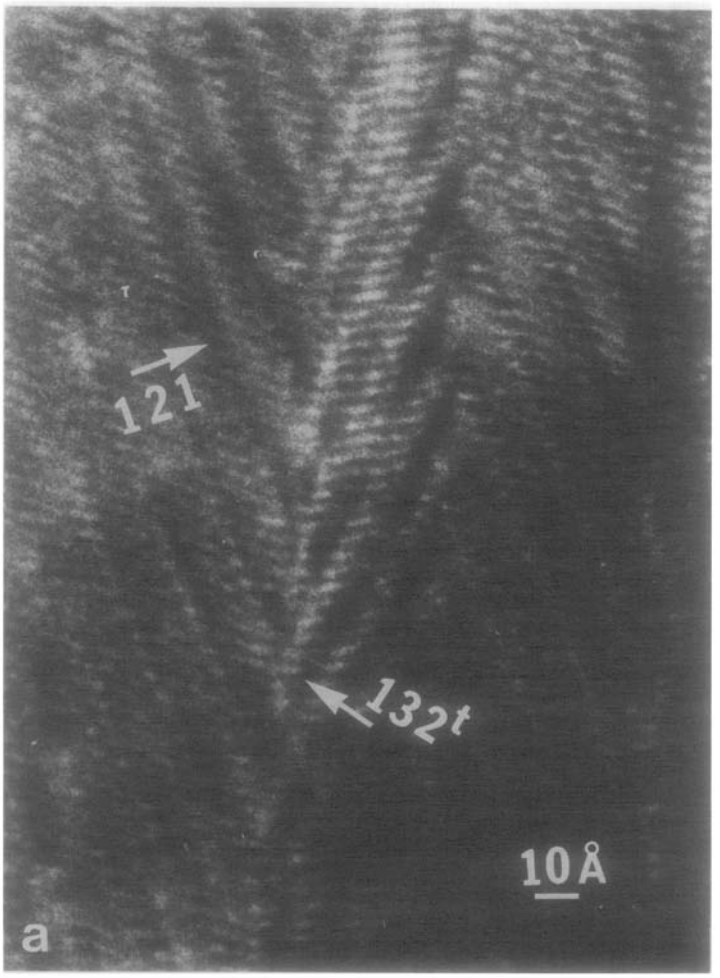

FIG. 6a. High-resolution image of a thick defect having an internal structure. The beam is in the [1$\bar{1}$1] orientation.

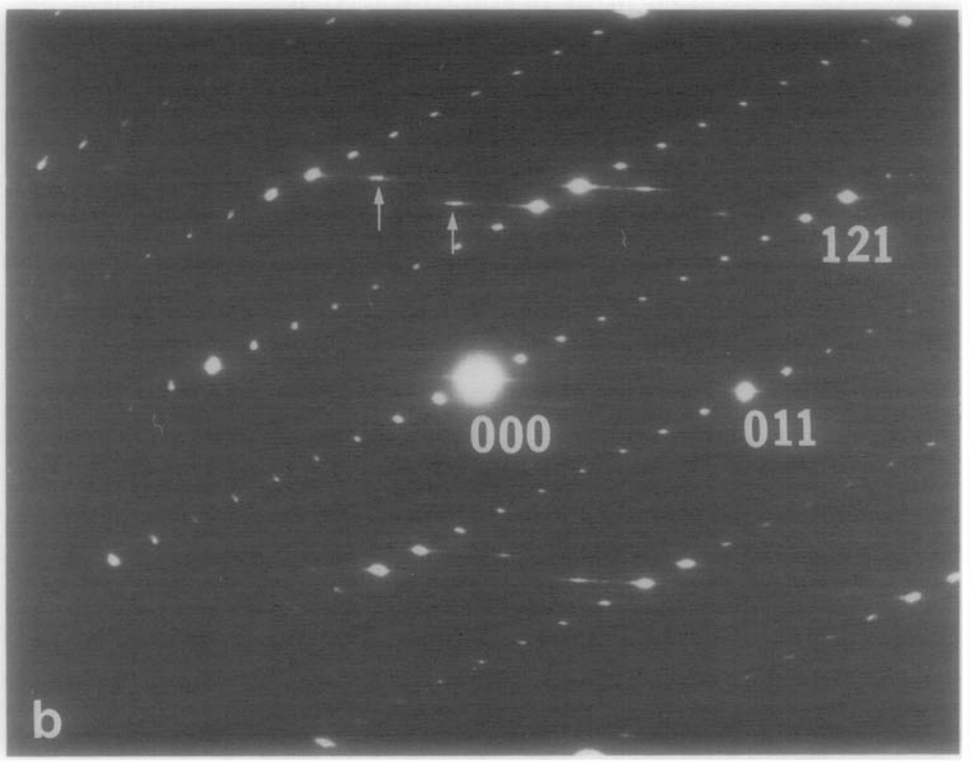

FIG. 6b. Diffraction pattern taken from the area shown in Fig. 6a. Arrows indicate intensity maxima due to ordered (132) *CS* planes.

the motion of jogs along the (011) plane and subsequently form thicker defects.

3. Thick faults are found to be in a twin relation with the matrix (with respect to the underlying VO_2 structure). Because a series of antiphase boundaries on every (011) anion plane generates a twin in a crystal with the rutile structure, such thick defects or microtwins are considered to be formed by a series of antiphase boundaries on every (011) anion plane. The structure in these twins is always the ordered *CS* structure with the (132) *CS* planes and not that with the (121) *CS* planes as in the matrix.

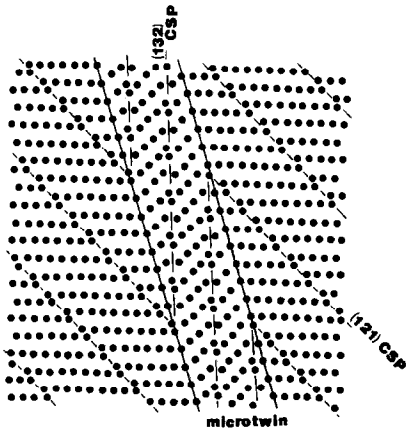

FIG. 7. Structure model of a thick defect (microtwin) with an internal structure. Continuous lines are boundaries between the matrix and the defect. Broken lines inside the defect represent the (132) *CS* planes.

It should be emphasized first that the appearance of the (011) defects is strongly related to the involvement of excess oxygen content beyond the strict stoichiometry of V_nO_{2n-1}, especially of V_9O_{17}. Single crystals of V_nO_{2n-1}, especially of n from 5 to 9, were routinely grown by vapor transport technique and their microstructures were investigated by transmission electron microscopy. Major defects in crystals grown

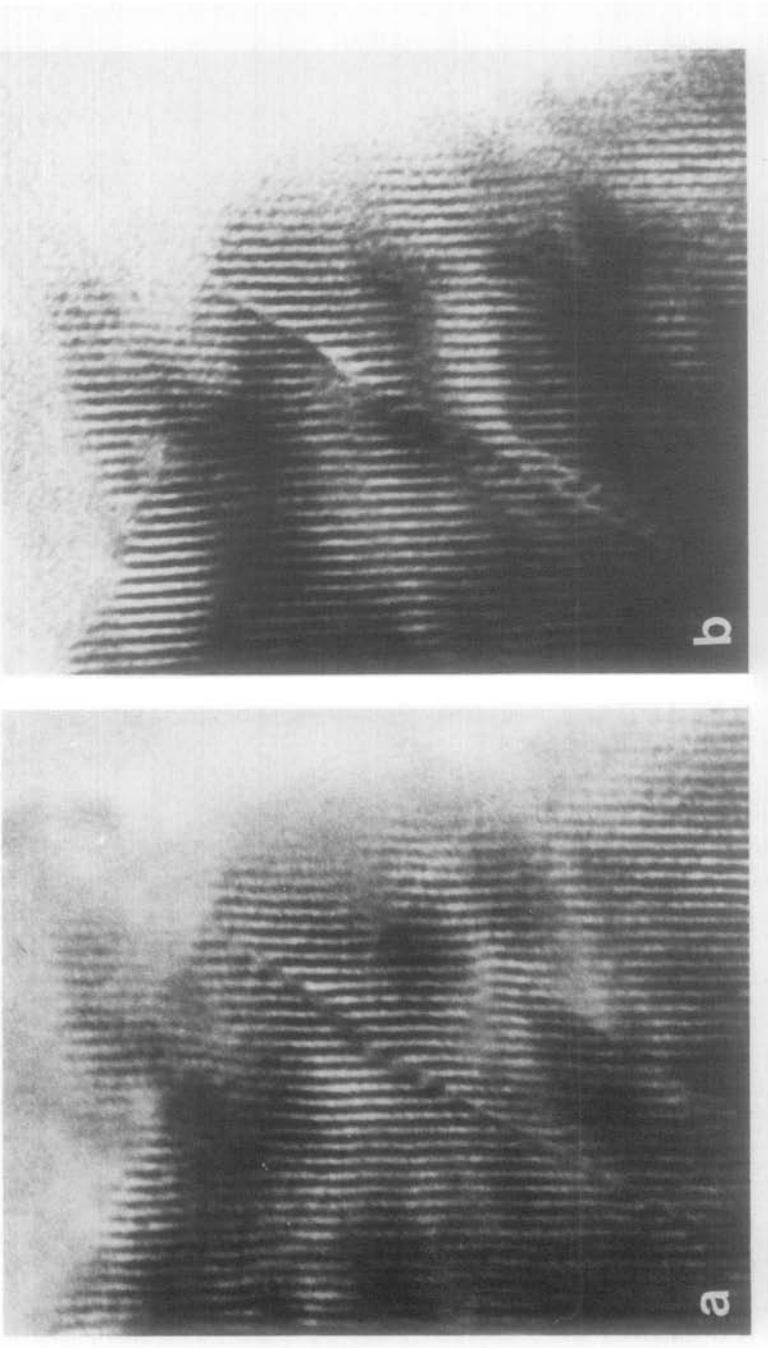

FIG. 8. Image of a bent defect showing its decomposition. (a) Image of a bent defect. (b) Image of the same defect which has decomposed into two components.

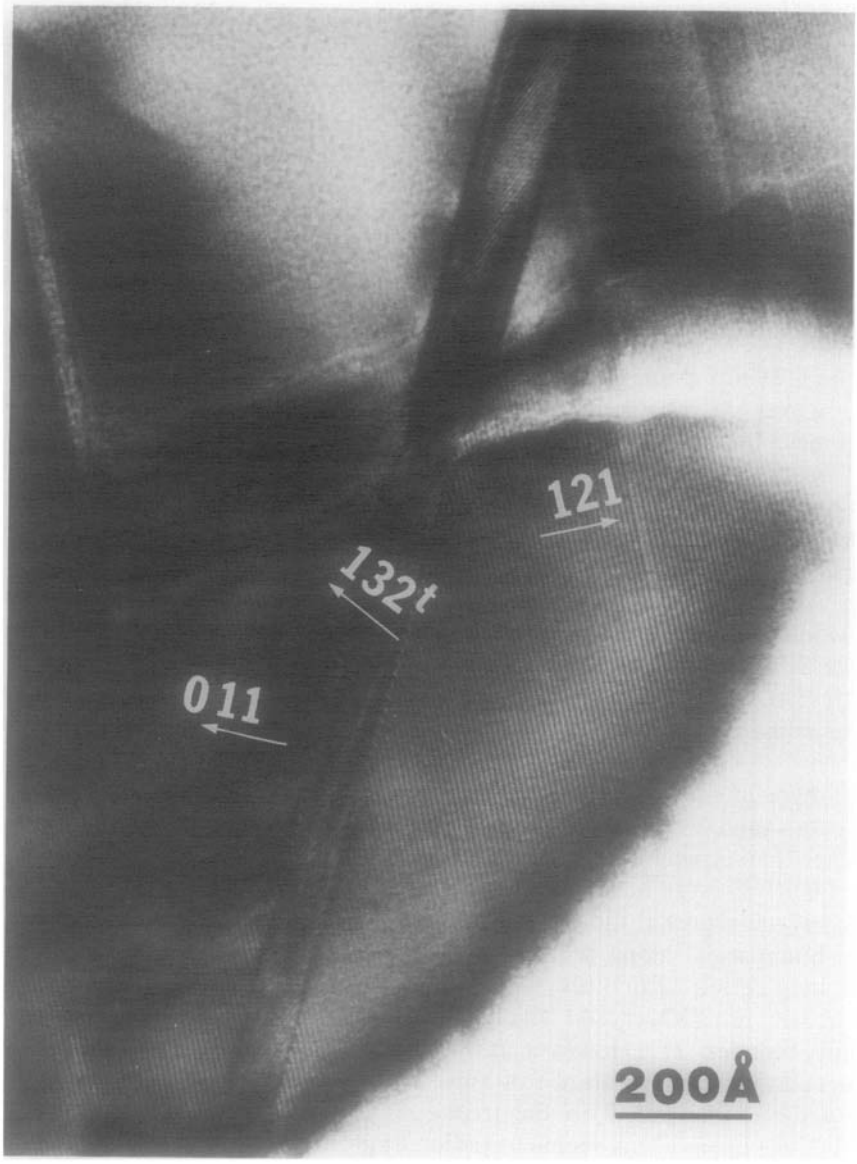

FIG. 9. Lattice image of a V_7O_{13} crystal showing a thick defect (microtwin) with ordered (132) *CS* planes. The beam is in the $[1\bar{1}1]$ orientation.

from materials having stoichiometric compositions are those connected to the microsyntactic intergrowth (*5, 9, 10*), especially when the growth rate is faster than the appropriate rate for individual compositions. Even for V_9O_{17}, if crystals are grown from a material having the stoichiometric composition and with slow enough growth rate, almost perfect crystals can be obtained (*5*). On the other hand, if crystals are grown from materials with excess oxygen content relative to V_9O_{17}, a high density of the (011) defects is observed, leading to the conclusion that the (011) defects are related to the involvement of the excess amount of oxygen in V_9O_{17}. Our main interest here then is to understand how these defects are related to excess oxygen content in V_nO_{2n-1} and

how the behavior of the V–O system is related to the Ti–O system with respect to the formation of series of long-period structures.

The antiphase boundary along the (011) plane, in view of its structure, should be among low-energy two-dimensional defects in the rutile structure and is observed in VO_2 and TiO_2. The existence of this type of defect is also expected in the Magnéli-phase compounds V_nO_{2n-1} or Ti_nO_{2n-1}. The existence of the (121) *CS* planes in these compounds, however, raises the energy of the (011) antiphase boundaries and this accounts, at least partially, for the appearance of this type of defect in Magnéli-phase compounds of longer periods. However, a drastic increase in the occurrence of the (011) defects in V_9O_{17} with excess oxygen cannot be understood from this trend only and the occurrence is also far more frequent and more distinct in appearance than in the corresponding composition range in the Ti–O system.

Indeed, there has been no report on the (011) defects, such as those observed in V_9O_{17}, other than typical antiphase boundaries in the Ti–O system. For example, Bursill and Hyde reported the existence of antiphase boundaries, along with a small group of long-period structures with the (132) *CS* planes, in a TiO_2 crystal which had been slightly reduced (*11*). However, it was also observed that the appearance of antiphase boundaries depended on the treatment of the specimens. This seems to indicate that the appearance of antiphase boundaries is due to strains created by rapid cooling. Not only is the appearance of the (011) defects in V_9O_{17} with excess oxygen different from ordinary antiphase boundaries, but their appearance does not depend on strain as shown by the present experiment. In other words, it can be concluded that the (011) defects in V_9O_{17} with excess oxygen are different in character from antiphase boundaries observed in the Ti–O system. On the other hand, Terasaki and Watanabe (*12*) and Anderson and Tilley (*13*) reported the appearance of [011]* streaks in diffraction patterns obtained from Ti_nO_{2n-1} crystals with the (121) *CS* planes. Although they did not obtain any images corresponding to these diffraction patterns, the streaks observed are similar to those in V_9O_{17} reported here and this may indicate that a similar type of defect can also appear in Ti_nO_{2n-1} to some extent.

We also observed some of the as-reacted particles which were used as starting specimens to grow crystals. Except for the fact that microsyntactic intergrowth of Magnéli phases of other periods was observed in these particles (which can be expected in specimens in a highly nonequilibrium state in growth as reported earlier) (*5*), the characteristics with respect to the (011) faults in V_9O_{17} were found to be essentially the same as those observed in single crystals produced under conditions close to equilibrium. As long as the composition of the material is close to stoichiometric, excessive (011) defects are not found.

The above observations strongly indicate that the (011) defects in V_9O_{17} are intrinsic defects characteristic of V_9O_{17} grown under the condition of excess oxygen. On the other hand, the (011) defect is essentially an antiphase boundary along the (011) plane and, if so, itself does not introduce any nonstoichiometry. However, the actual (011) defects observed in V_9O_{17} are not simply antiphase boundaries but they include a large number of defects: they are not straight, involve steps, and are thick with varying widths. This fact leads to a conclusion that a series of (low energy) antiphase boundaries is created in order to introduce defects which can accommodate excess oxygen content in V_9O_{17} rather than to create (energetically more costly) long-period structures such as those observed in the Ti–O system in the composition range between $Ti_{10}O_{19}$ and TiO_2. To illustrate these concepts, projections of defects (antiphase boundary) with steps are shown in Fig. 10.

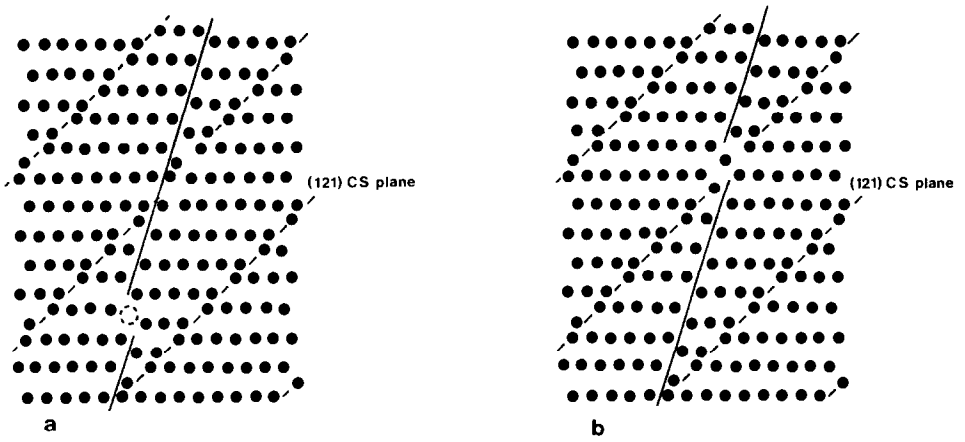

FIG. 10. Structure model of a defect (antiphase boundary) having a step. (a) A step in the center of two *CS* planes. (b) A step at the intersection of the antiphase boundary and the *CS* plane.

Figure 10a shows an antiphase boundary with a step between the two *CS* planes, while Fig. 10b shows an antiphase boundary with a step at the intersection with a *CS* plane. Both create a missing metal site and hence introduce nonstoichiometry. However, energetically the latter is preferred from its geometry and, hence, the explanation is given for the latter case. It can be seen that a pair of vanadium ions at the *CS* plane disappears at the step and a change of composition toward VO_2 occurs. If such a step is created at every intersection with the *CS* plane, the total amount of bending of an antiphase boundary is about 5°, in agreement with observation.

The existence of steps in antiphase boundaries is still energetically costly and there should be a tendency to eliminate these steps if the specimen is annealed. We have often observed such motions of steps during TEM observation. This motion is probably created by heating due to the electron beam. An example is shown in Fig. 8. A defect after such a step has moved along the (011) plane is shown in Fig. 8b. This motion would eventually drive excess oxygen out of the specimen, leading the specimen toward the stoichiometric composition, V_9O_{17}. It is thus believed that this is, at least, one mechanism of creating thick (011) defects, and that defects observed in V_9O_{17} grown from specimens with excess oxygen content are the results after the excess oxygen content has been eliminated by annealing. In other words, the excess oxygen content in crystals observed can be far smaller than the composition of the starting materials might indicate. If such a motion of jogs occurs along consecutive (011) planes, this would create microtwin bands in the specimen. We believe that microtwin bands observed in V_9O_{17} and in other Magnéli-phase compounds are created in this fashion.

Microtwin bands (with respect to the underlying VO_2 structure) in V_nO_{2n-1} have long-period structures with the (132) *CS* planes (Figs. 6, 9). Important features of the (132) *CS* structure in microtwin bands in V_nO_{2n-1} are that the period is exactly the same as that of the (121) *CS* structure of the matrix and that the (132) *CS* planes are geometrically related to the (121) *CS* planes of the matrix as explained earlier. The exclusive appearance of the (132) *CS* structure in the microtwin with the same period as the (121) *CS* structure in the matrix is hard to explain thermodynamically. Therefore, the formation of the (132) *CS* structure in V_nO_{2n-1} is to be interpreted as a natural consequence of the twin formation, and hence is different in origin from the formation of the (132) *CS* structure in the Ti–O

system which are introduced to compensate for the nonstoichiometry in the composition range beyond $Ti_{10}O_{19}$.

The following general characteristics of the long-period modulation of crystals might be helpful in understanding the difference. The stability of a homologous series of long-period structures with respect to the fundamental structure (the structure from which a particular series of long-period structures is derived by modulation or the modulated structure with period infinity) is conveniently discussed as a competition of the stabilization free energy to form the long-period structure and the boundary free energy required for the modulation (*14, 15*). If the boundary energy to create the modulation is larger than the stabilization energy, the formation of that particular long-period structure is suppressed. Both free energy terms depend on the period. The stabilization energy is larger as the period becomes shorter, but it decreases faster than linearly with inverse period as the period becomes larger (as the structure approaches the fundamental structure), whereas the boundary energy decreases linearly (*14, 15*). Therefore, this leads to a natural long-period limit. In the present case of the Magnéli structure, the fundamental structure is the rutile structure and the modulation is due to the (121) *CS* plane. Apparently, the (121) *CS* plane is the lowest energy modulation plane (or the boundary) in view of the existence of stable V_nO_{2n-1} or Ti_nO_{2n-1}. Based on this modulation mode, V_9O_{17} and $Ti_{10}O_{19}$ are the structures with the longest periods. However, if the (132) *CS* plane is utilized as the modulation plane, the same stoichiometry (or the period) can be achieved with a shorter distance between the *CS* plane. This means that as n becomes larger in V_nO_{2n-1} or Ti_nO_{2n-1}, the structure with the (132) *CS* plane is more favorable with respect to the stabilization energy and, hence, the structure with the (132) *CS* plane can take over in structures with larger n if the (132) boundary energy is favorable. Therefore, in the composition range between $Ti_{10}O_{19}$ and TiO_2, the appearance of long-period structures with the (132) *CS* plane (and also with the *CS* plane of orientations between the (121) plane and the (132) plane) is considered to be due to a favorable (132) boundary energy in the Ti–O system.

The nonappearance of similar structures in the V–O system is then simply attributed to the unfavorable size of the (132) boundary energy with respect to the stabilization energy. It can, however, be that the stabilization energy of the (132) *CS* structure in the V–O system is more favorable than the (121) *CS* structure in the structure with relatively large n. The exclusive appearance of the (132) *CS* structure in microtwins but with the same period as in the matrix of the (121) *CS* structure thus indicates that the *CS* structure in the twin is formed under the condition in which the contribution of the boundary energy can be disregarded. A possibility is suggested below.

The amount of shift involved in creating the antiphase boundary along the (011) plane in VO_2 is given by $\frac{1}{2}$ $[0\bar{1}1]$ or its odd multiple. On the other hand, in order to create the (121) *CS* structure in the twin formed by a series of antiphase boundaries on every (011) anion plane, a shift of $\frac{5}{2}$ $[0\bar{1}1]$ per antiphase boundary is required, and for creating the (132) *CS* structure, the shift involved is $\frac{7}{2}$ $[0\bar{1}1]$ per antiphase boundary. As indicated above, the (132) *CS* structure in the V–O system may be more favorable with respect to the stabilization energy than the (121) *CS* structure with n as low as 7. It seems, therefore, that the choice of the shift per antiphase boundary in forming twins is solely determined by the magnitude of the stabilization energy of existing *CS* structure when such microtwin bands are formed by the motion of jogs along consecutive (011) planes.

A considerable amount of effort has been spent on the stability of the *CS* structure (*16–18*). Most efforts are to calculate the

stability by directly comparing the disordered and the ordered *CS* structures in the Ti–O and the V–O systems. Also, discussions have been made with respect to the relationship between *CS* plane orientations and the anisotropy in Young's modulus (*19*). Although the problems are not unrelated, it is hard to apply these arguments directly to the present problem.

Acknowledgments

We thank Professor J. M. Honig of the Chemistry Department for his valuable discussions and comments. This work was supported by NSF MRL Grant DMR-77-23798. Equipment provided through an NSF grant DMR-78-09025 was crucial for the success of this work.

References

1. H. Horiuchi, N. Morimoto, and M. Tokonami, *J. Solid State Chem.* **17,** 407 (1976).
2. L. A. Bursill and B. G. Hyde, *in* "Prog. in Solid State Chemistry" (A. Reiss and J. O. McCaldin, Eds.), Vol. 7, p. 177, Pergamon, Oxford (1972).
3. K. Kosuge, H. Okinaka, S. Kachi, K. Nagasawa, Y. Bando, and T. Takada, *Japan. J. Appl. Phys.* **9,** 1004 (1970).
4. J. R. Gannon and R. J. D. Tilley, *J. Solid State Chem.* **25,** 301 (1978).
5. H. Kuwamoto, N. Otsuka, and H. Sato, *J. Solid State Chem.* **36,** 133 (1981).
6. S. Anderson, *Acta Chem. Scand.* **14,** 1161 (1960).
7. L. A. Bursill, B. G. Hyde, O. Terasaki, and D. Watanabe, *Philos. Mag.* **20,** 347 (1969).
8. Y. Bando, S. Muranaka, Y. Shimada, M. Kyoto, and T. Takada, *J. Cryst. Growth* **53,** 443 (1981).
9. Y. Hirotsu, S. P. Faile, and H. Sato, *Mater. Res. Bull.* **13,** 895 (1978).
10. Y. Hirotsu and H. Sato, *Mater. Res. Bull.* **15,** 41 (1980).
11. L. A. Bursill and B. G. Hyde, *Proc. Roy. Soc. London Ser. A* **320,** 147 (1970).
12. O. Terasaki and D. Watanabe, *Japan. J. Appl. Phys.* **10,** 292 (1971).
13. J. S. Anderson and R. J. D. Tilley, *J. Solid State Chem.* **2,** 472 (1970).
14. H. Sato and R. S. Toth, *Phys. Rev.* **124,** 1833 (1961).
15. H. Sato and R. S. Toth, "Alloying Behavior in Concentrated Solid Solutions" (T. B. Massalski, Ed.), p. 293, Gordon & Breach, New York (1965).
16. A. M. Stoneham and P. J. Durham, *J. Phys. Chem. Solids* **34,** 2127 (1973).
17. C. R. A. Catlow, "AIP Conference Proceedings No. 53, Modulated Structures 1979," (J. M. Cowley, J. B. Cohen, M. B. Salamon, and B. J. Wuensch, Eds.), p. 149 (1979).
18. Y. Shimizu and E. Iguchi, *Phys. Rev. B* **17,** 2505 (1978).
19. L. A. Bursill, D. J. Netherway, and I. E. Grey, *Nature (London)* **272,** 405 (1978).